CHAPTER 4 RESULTS AND DISCUSSION

Although glasses can be made by a wide variety of methods, the vast majority are still produced by heat treatment and batch component at an elevated temperature. This procedure always involves the selection of raw materials, batch calculations, weighing and mixing materials to provide a homogenous and heating process, etc. A measurement and analysis glass sample is the importance process for physical, structural, optical, radiation shielding and luminescence properties of glasses. The aim of this research was to study and characterize the properties of zinc bismuth borate glasses and investigate Eu^{3+} ion doped in zinc bismuth borate glasses.

4.1 Zinc Bismuth Borate Glass Samples

4.1.1 General Characteristic of Glass Samples

The series of zinc bismuth borate glasses prepared in composition ($10ZnO : xBi_2O_3 : (90 - x)B_2O_3$ (where x = 15, 20, 25 and 30 mol %) using a melt quenching technique. Chemical powers of analytical reagent consisted of ZnO, Bi_2O_3 and H_3BO_3. All chemical composition was finely powder and then mixed in whole of composite. Batches for producing 30 g of glass were melted in high alumina crucibles in an electric furnace at 1,100 $^{\circ}$C with soaking time for 3 hours under normal atmospheric conditions. Afterwards, the melts were quickly poured onto a preheated stainless steel plate and pressed to a thickness of approximately 0.5 mm by another plate, annealed at 500 $^{\circ}$C for 3 hours and slowly cooled down to room temperature, respectively. Finally, the as-prepared glass samples were cut and then finely polished to a dimension of 1.0 cm x 1.5 cm x 0.3 cm. The chemical compositions of ZnO - Bi_2O_3 - B_2O_3 (ZBB) glasses prepared in the present study are given in Table 4.1. The homogeneous glass samples for all compositions of zinc bismuth borate are optically transparent and are illustrated in Figure. 4.1. The intensity of yellow color of glasses was increased with increasing Bi_2O_3 content.

Table 4.1 Chemical compositions of the zinc bismuth borate glasses (in mol %).

Samples no.	Bi_2O_3 (mol%)	Glass formula
1	15	$10ZnO:15Bi_2O_3:75B_2O_3$
2	20	$10ZnO:20Bi_2O_3:70B_2O_3$
3	25	$10ZnO:25Bi_2O_3:65B_2O_3$
4	30	$10ZnO:30Bi_2O_3:60B_2O_3$

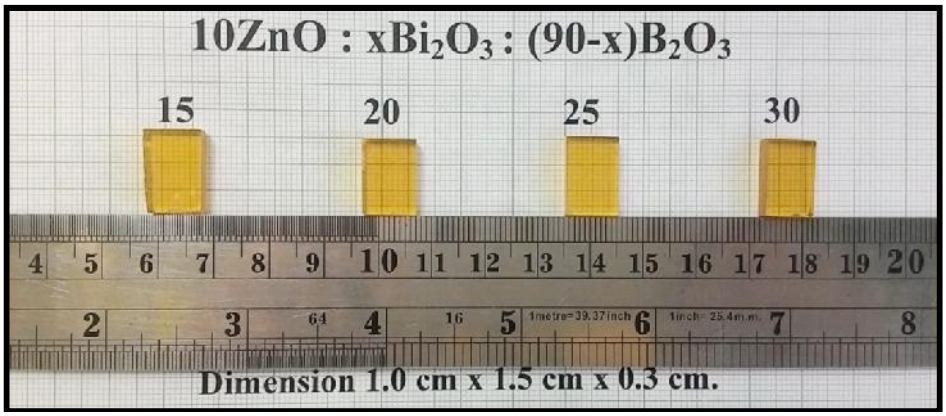

Figure 4.1 Photographs of the as - prepared zinc bismuth borate glass samples.

4.1.2 Density, Molar Volume and Vicker's Hardness of glass samples

The determined density (ρ) of the glass samples and the molar volume (V_M) of the glass samples are included in Table 4.2. The ZBB glasses show high density due to present of high Bi_2O_3. The variations of density and hardness (in Vicker's scale) with composition of Bi_2O_3 are shown in Figures 4.2 and 4.3, respectively. It is evident from Table 4.2 that the density of the result present glass system increases with increase in of Bi_2O_3 content. This is due to the high relative molecular mass of Bi_2O_3 compared to other glass constituents. In general trend, the molar volume (V_M) and hardness of the glasses increases with increase in Bi_2O_3 content. The molar volume of the glasses increases due to increase in bond length or inter atomic spacing. It has happen due to the higher ionic radius of Bi^{3+} (0.102 nm) than that of other glass former ions (Zn^{2+} = 0.083nm, B^{3+} = 0.020 nm). Therefore, it can understand that V_M as the volume corresponding structural unit with it surrounding space will increase by insertion of Bi_2O_3.

Table 4.2 The values of density (°), molecular weight (M_T) and molar volume (V_M) of ZBB glass samples.

Sample No.	Glass formula (mol%)	Density ° (g/cm^3)	Molecular weight M_T (g/mol)	Molar volume V_M (cm^3/mol)
1	$10ZnO:15Bi_2O_3:75B_2O_3$	3.247±0.0017	130.20	40.90
2	$10ZnO:20Bi_2O_3:70B_2O_3$	3.475±0.0024	150.10	43.50
3	$10ZnO:25Bi_2O_3:65B_2O_3$	3.980±0.0059	169.90	43.30
4	$10ZnO:30Bi_2O_3:60B_2O_3$	4.129±0.0054	189.70	46.20

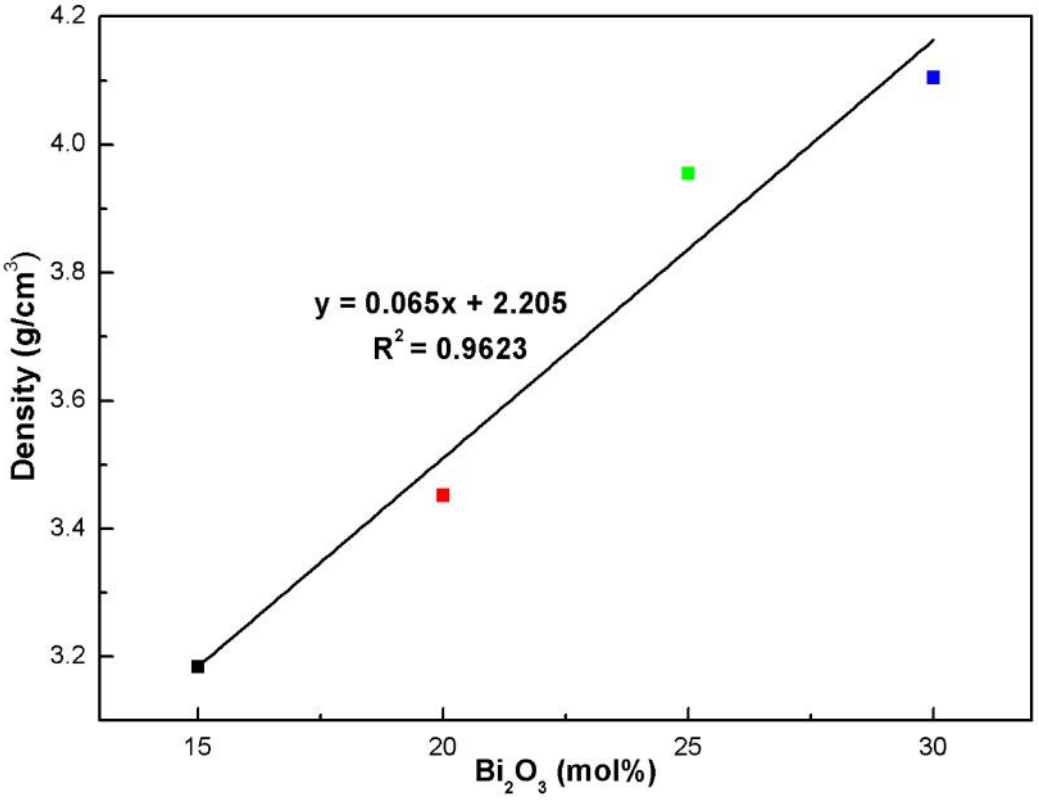

Figure 4.2 Densities of ZBB glasses doped with different Bi_2O_3 concentrations.

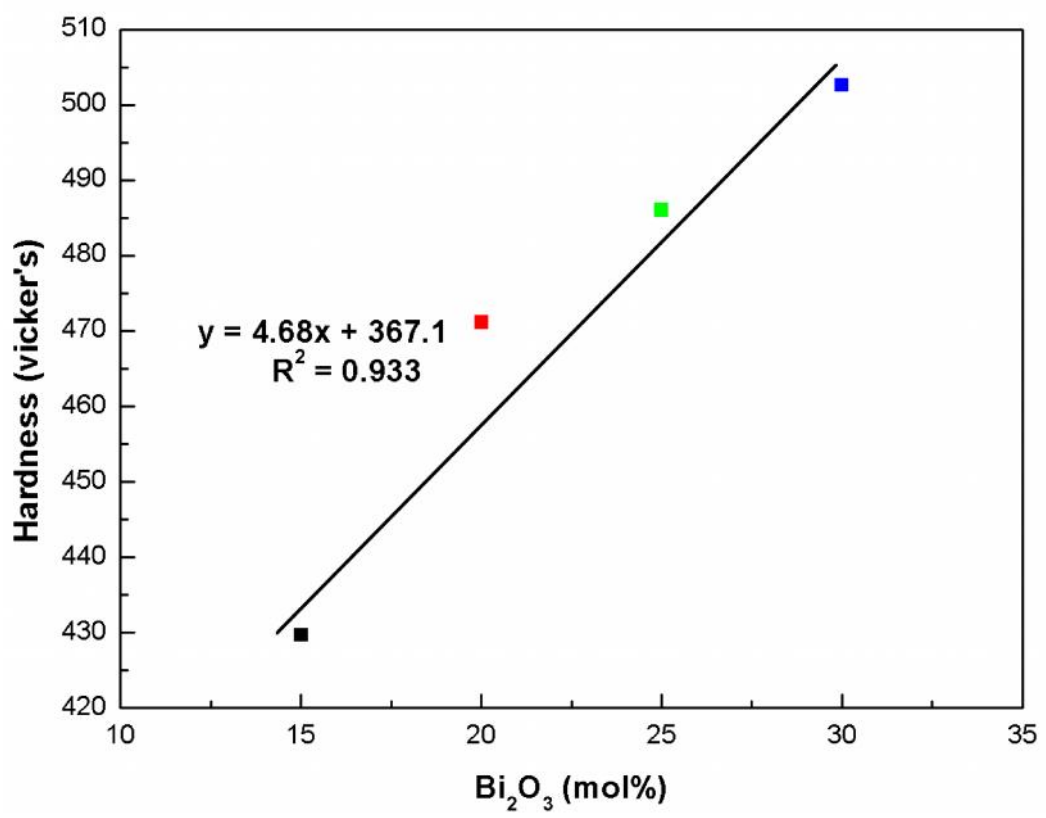

Figure 4.3 Vicker's hardness of ZBB glasses doped with different Bi_2O_3 concentrations.

4.1.3 Gamma - Ray Shielding Properties

The mass attenuation coefficients of ZBB glass of different Bi_2O_3 concentration measured at different gamma ray energies are shown in Table 4.3. The experimental values of mass attenuation coefficients were evaluated from intensities of incident (I_0) and transmitted (I) gamma - ray at a selected energy level. The theoretical values of mass attenuation coefficients for all glass compositions and energies were calculated from WinXCom program.

It has been found that the total mass attenuation coefficients of all the ZBB glasses were decreased exponentially with the increasing of gamma ray energy, which indicates the increasing of total interaction. These trends were observed in the glasses for all Bi_2O_3 concentrations. In the following figures, line-style followed by number mol% (th) will be used to signify the theoretical values while point-style followed by number mol% (ex) signifies the experimental values. There are good agreements on the mass attenuation coefficients obtained experimentally and theoretically as shown in Figure 4.4. The errors between the experimental and theoretical values could mainly be attributed to the non - stoichiometry in the glass formula as a result of high melting temperature. In Figure 4.5, the total mass attenuation coefficients of the glasses are observed over Bi_2O_3 concentrations for the Compton scattering energies. The total mass attenuation coefficients are increased with the increase of Bi_2O_3 concentrations for all energies. The effect of Bi_2O_3 concentration on the total mass attenuation coefficients can easily be observed at lower energy; e.g. higher slope for the low energy line at 223.02 keV than the high energy line at 662 KeV. This result is due to different partial interactions contributed by different Bi_2O_3 concentrations in the glass samples.

Table 4.3 The mass attenuation coefficients of ZBB glasses of different Bi_2O_3 concentrations at different gamma ray energies.

Energy (keV)	$[Bi_2O_3]$ = 15 mol%			$[Bi_2O_3]$ = 20 mol%			$[Bi_2O_3]$ = 25 mol%			$[Bi_2O_3]$ = 30 mol%		
	$\mu_{m(th)}$ ($x10^{-2}$ cm^2/g)	$\mu_{m(ex)}$ ($x10^{-2}$ cm^2/g)	%RD	$\mu_{m(th)}$ ($x10^{-2}$ cm^2/g)	$\mu_{m(ex)}$ ($x10^{-2}$ cm^2/g)	%RD	$\mu_{m(th)}$ ($x10^{-2}$ cm^2/g)	$\mu_{m(ex)}$ ($x10^{-2}$ cm^2/g)	%RD	$\mu_{m(th)}$ ($x10^{-2}$ cm^2/g)	$\mu_{m(ex)}$ ($x10^{-2}$ cm^2/g)	%RD
223.02 ±12.2	44.73	44.32 ±2.25	0.92	49.87	49.32 ±2.37	1.10	53.85	54.12 ±2.43	0.50	56.97	56.77 ±2.51	0.35
252.98 ±14.2	34.81	34.29 ±2.02	1.49	38.49	38.95 ±1.98	1.20	41.34	40.87 ±2.04	1.14	43.58	43.88 ±1.99	0.69
287.28 ±15.6	27.54	28.02 ±1.48	1.74	30.17	30.25 ±1.62	0.27	32.20	32.71 ±1.72	1.58	33.80	34.14 ±1.63	1.01
340.83 ±16.1	20.72	21.05 ±1.01	1.59	22.39	22.58 ±1.14	0.85	23.69	23.28 ±1.11	1.73	24.71	24.78 ±1.07	0.28
398.97 ±16.0	16.44	16.67 ±0.67	1.40	17.55	17.29 ±0.85	1.48	18.40	18.17 ±0.73	1.25	19.07	18.86 ±0.81	1.10
481.59 ±20.7	12.95	12.83 ±0.53	0.93	13.62	13.54 ±0.62	0.59	14.14	14.32 ±0.72	1.27	14.55	14.63 ±0.77	0.55
562.68 ±27.8	10.92	10.99 ±0.35	0.64	11.36	11.58 ±0.34	1.94	11.70	11.75 ±0.39	0.43	11.97	11.82 ±0.42	1.25
662.00 ±18.1	9.332	9.415 ±0.287	0.89	9.614	9.588 ±0.276	0.27	9.832	9.798 ±0.311	0.35	10.00	10.07 ±0.36	0.70

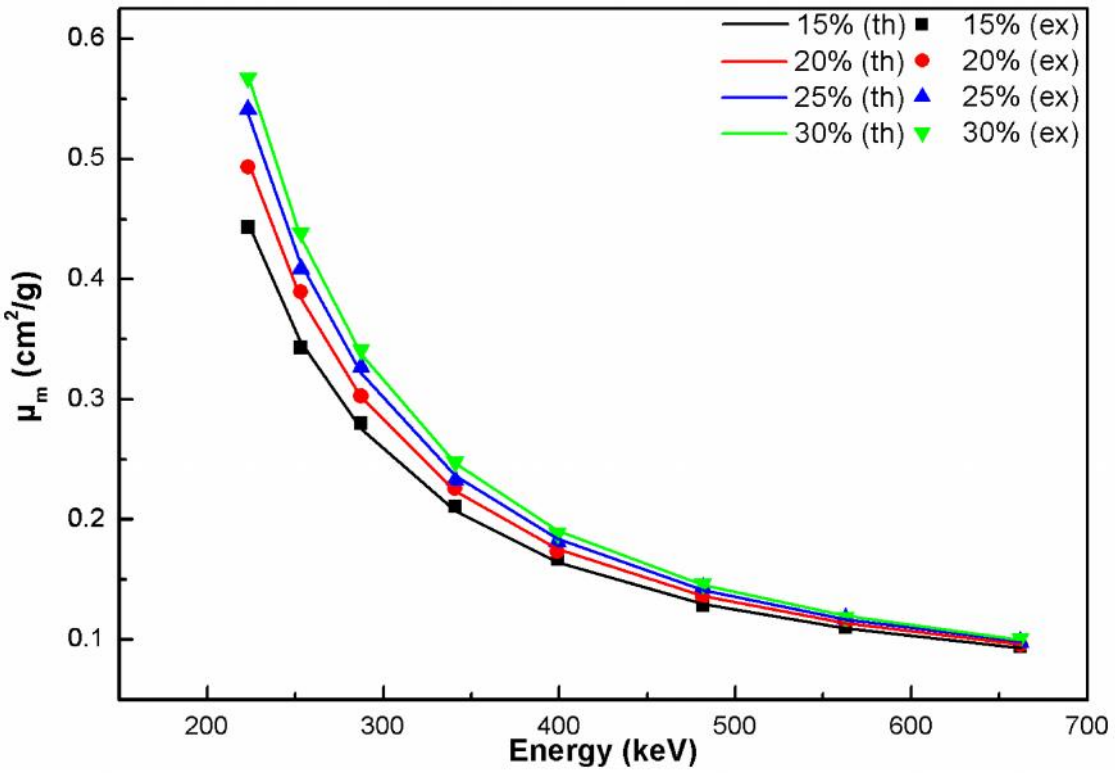

Figure 4.4 Experimental and theoretical values of the total mass attenuation coefficients of ZBB glasses at different energies.

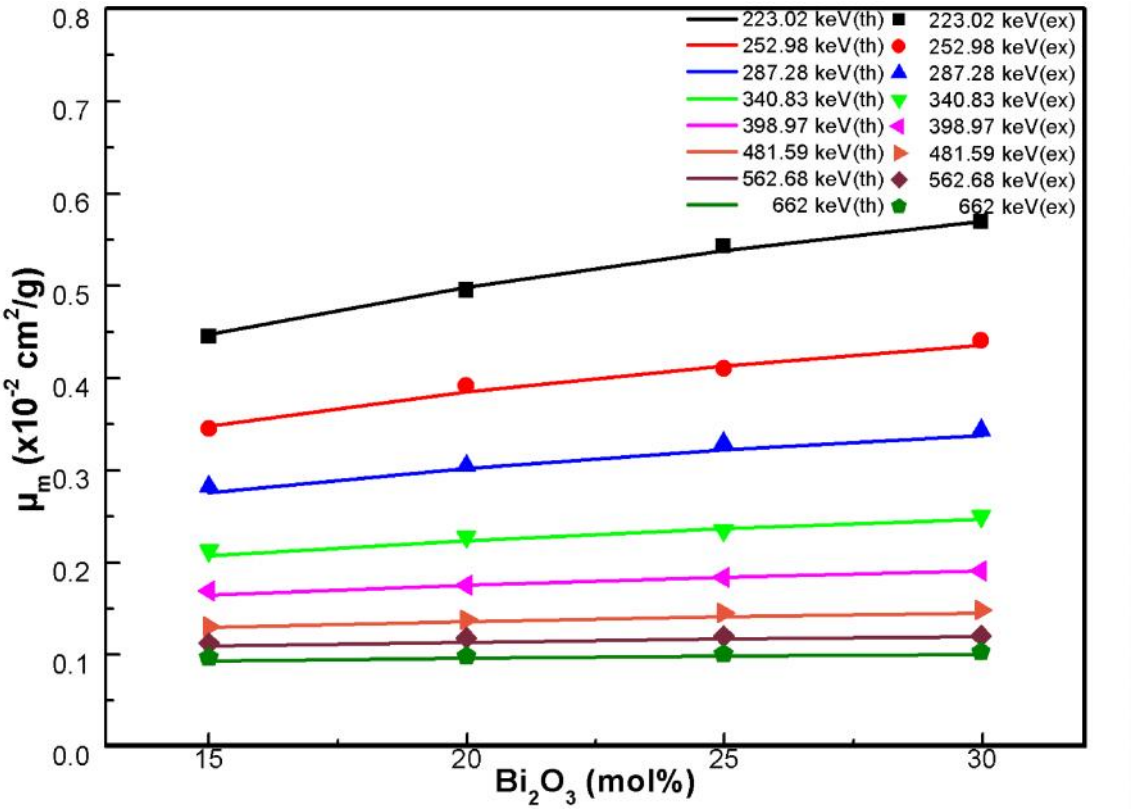

Figure 4.5 Experimental and theoretical values of the total mass attenuation coefficients of ZBB glasses of different Bi_2O_3 concentrations.

The effective atomic number (Z_{eff}) of the ZBB glasses were calculated using equation (4.1)

$$Z_{eff} = \frac{\pm_{t,a}}{\pm_{t,el}} \tag{4.1}$$

and the results are shown in Figure 4.6. It is seen that the value of the Z_{eff} were decreased with the increasing of gamma ray energies. There are good agreements between experimental and theoretical values. Several experimental results published had found similar findings on the dependent of Z_{eff} on the photon energy such are thermoluminescence materials [97], alloy [98-99], superconductor [100], semiconductor [101] and biological materials [102].

The variation of effective electron densities (N_e) of ZBB glasses at different gamma ray energies is shown in Figure 4.7. The ZBB glasses show with higher N_{el} values at low energy then decrease exponentially toward high energy. This indicates there are more interactions of ZBB glasses with gamma - rays of low energies than high energies and hence more electrons as the results are generated at low energy. The N_e results are observed with similar trends to Z_{eff}, both values are decreased exponentially toward high energies.

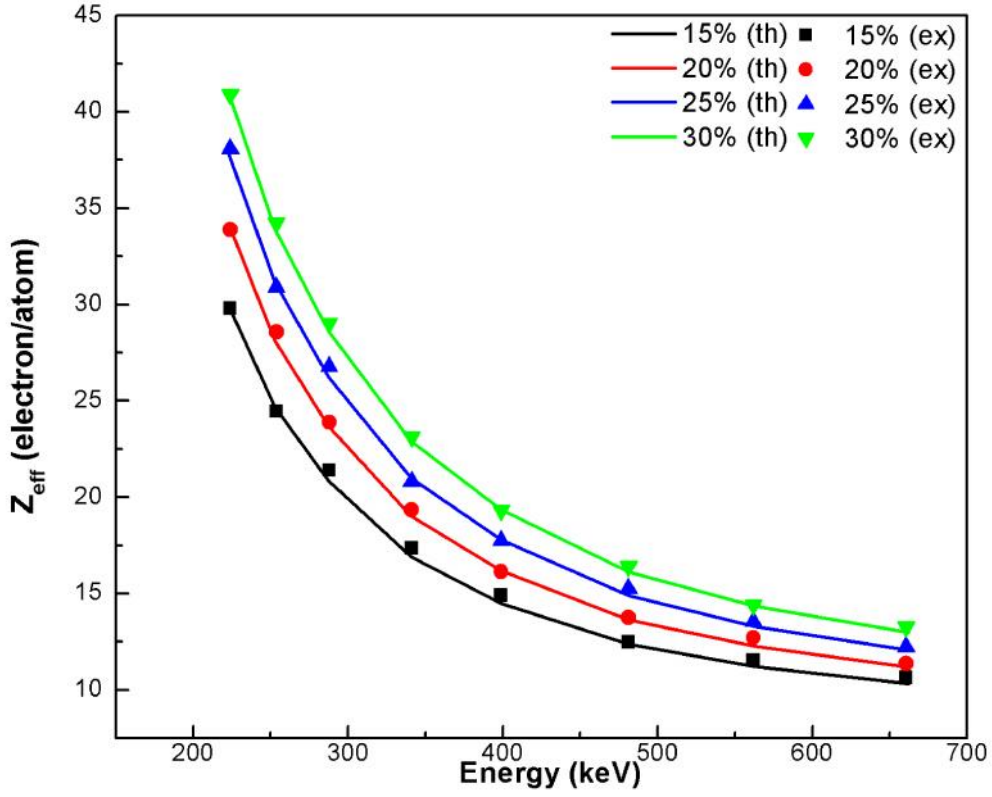

Figure 4.6 Experimental and theoretical values of the effective atomic numbers of ZBB glasses at different energies.

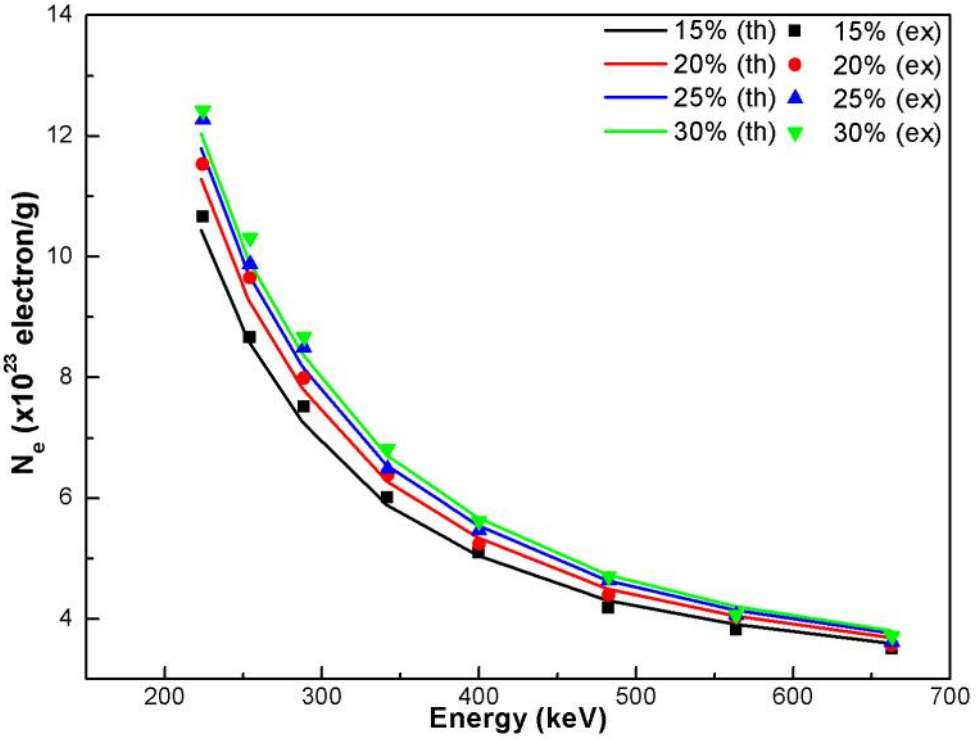

Figure 4.7 Experimental and theoretical values of the effective electron densities of ZBB glasses at different energies.

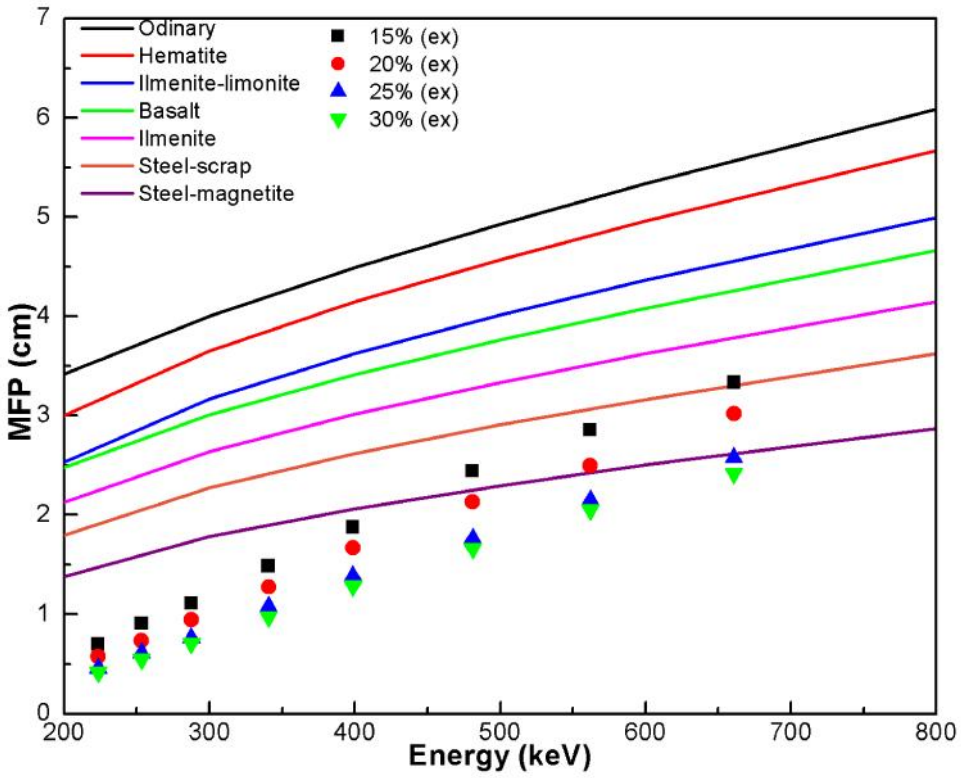

Figure 4.8 The photon mean free path of ZBB glasses at different energies compared with WinXCom results on some standard shielding materials.

Figure 4.8 shows the photon mean free path (MFP) values of ZBB glasses at different energies compared with WinXCom results on some standard shielding materials. The compositions and densities of standard shielding materials were obtained from literature [103]. The compositions were used for μ_m calculation by WinXCom. The linear attenuation coefficients (μ) was obtained from $\mu = \mu_m \rho$. Finally, the MFP were calculated using relation MFP = 1/u. The MFP represents the averaged travel distance between two successive photo interactions. The shorter MFP indicates more interaction of photons to material and hence posses the better shielding properties [104]. In this work, MFP is longer with increasing of gamma ray energies, reflecting that more penetrating power of gamma-rays at higher energy.

In order to test for practical usage, it is necessary to compare the MFP of the glasses to some standard shielding concretes. It can be seen from Figure 4.9, the steel - magnetite concrete performs the best as standard shielding material in the studied energy range. The ZBB glasses developed in this work with Bi_2O_3 content in the glass samples higher than 25 mol % (25 and 30 mol %) show lower MFP values against all the standard shielding concretes over the entire energy range. These results are good indications that the ZBB glasses in the present study may be developed as radiation shielding materials.
For the glasses containing Bi_2O_3 of 15 and 20 mol %, they exhibit better shielding properties than steel-magnetite concrete only at energy below 398 keV and 481 keV, respectively.

4.1.4 Amorphous Nature of Glass Samples

The amorphous nature of ZBB glasses doped with different Bi_2O_3 concentrations was confirmed by X - ray diffractometer from Cu (K_α, λ = 1.5406 Å) with an angular range 20 - 80 (2θ) degree with a step length of 0.02 degree and a counting time 60 sec/step. X - ray diffraction patterns of all glass samples show a hump were observed in the 2θ about 30 degree, indicating disordered structure and amorphous nature of glass samples. The XRD patterns of ZBB glasses doped with different Bi_2O_3 concentrations are shown in Figure 4.9.

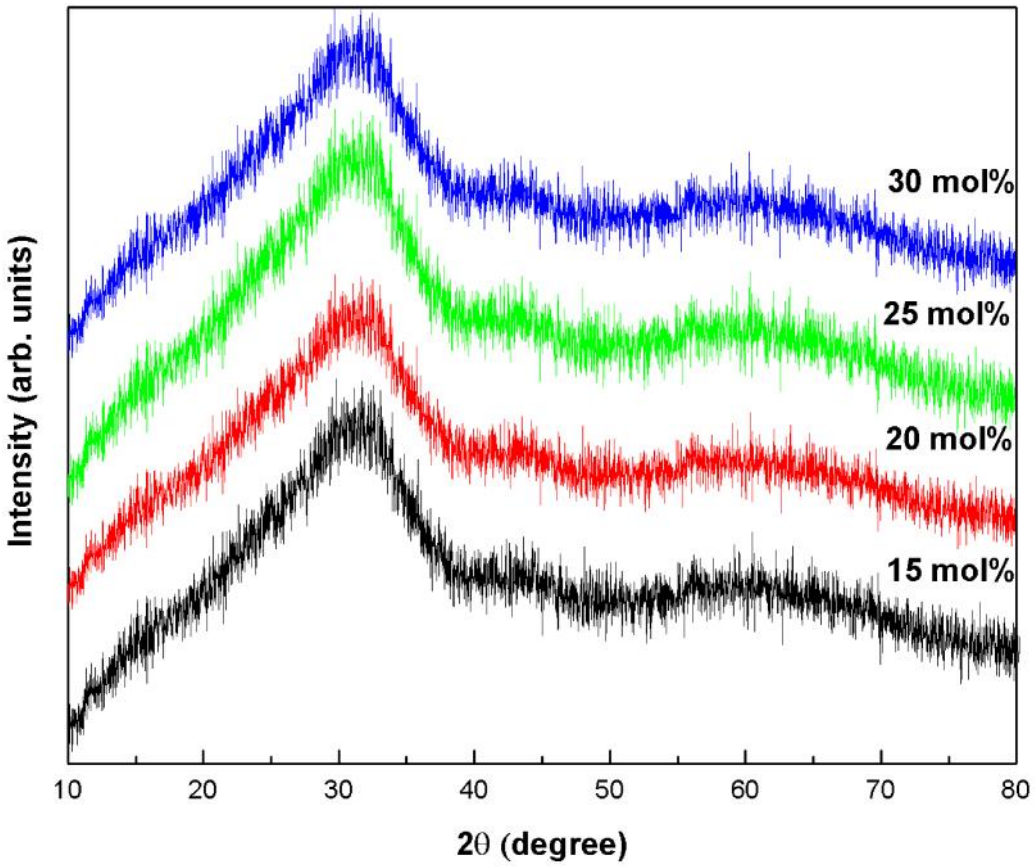

Figure 4.9 Diffraction patterns of ZBB glasses doped with different Bi_2O_3 concentrations.

4.1.5 FTIR Transmittance Spectra

The infrared spectra of xBi_2O_3 :10ZnO : (90 - x)B_2O_3 glass system (where x = 15, 20, 25 and 30 mol %) is displayed in Figures 4.10. According to Krogh - Moe model, the structure of borate glass consists of BO_3 triangles with certain fraction of six membered (boroxol) rings [105]. In B_2O_3 glasses boron [B^{3+}] ion are triangularly coordinated by oxygen to form glasses easily. The BO_3 triangles are corner bonded in a random network [106]. The introduction of transition metal ions in these glasses helps the boron to form tetraborate groups and progressive substitution of boroxal rings by triborate and tetraborate groups [107]. The boroxal ring shows its characteristic frequency at 806 cm^{-1} and the presence or absence of this band decides the existence or absence of boroxal rings in the structure. In the present set of glasses no band was observed at or around 806 cm^{-1} indicating that no boroxol rings are present in these glasses.

The peaks of the IR spectra of the glasses under study are listed in Table 4.4. The bands observed in the region 2080 - 2940 in all the glass samples are attributed to the hydroxyl or water group [108]. The present set of glasses show transmission bands in regions 2904, 2830, 2287, 2080, 1268, 996, 848, 766 and 651 cm^{-1}. It has been reported that the bands observed in the region 1268 cm^{-1} are due to the asymmetrical stretching relaxation of the B - O bond of trigonal BO_3 units [109]. The band around 996 cm^{-1} originates from B - O bond stretching of the tetrahedral BO_4 units and is due to the vibration of some boron atoms attached to the non-bridging oxygen in the form of BO_4 vibrations [110]. The shoulder around 840 cm^{-1} is related to the symmetrical stretching vibration of Bi - O in [BiO_3] group [111]. The band around 766 cm^{-1} is the bending mode of = B – O – B ≡ bonds in which oxygen bridges between one tetrahedral and one trigonal boron atom [112]. The band observed around 651 cm^{-1} is the bond bending mode of B - O - B vibrations [113-114]. In the IR spectra of the present glass system it was found that the incorporation of ZnO does not show much effect on the structure of the glasses under study. The addition of ZnO in the present glass system produces a very small change in the IR bands that do not account for the major structural changes. However, in many glass systems in which ZnO is a major constituent the possibility of formation of ZnO_4 may be more [115]. S. Bale et al. have reported the formation of ZnO_4 units with increase in zinc oxide content [116].

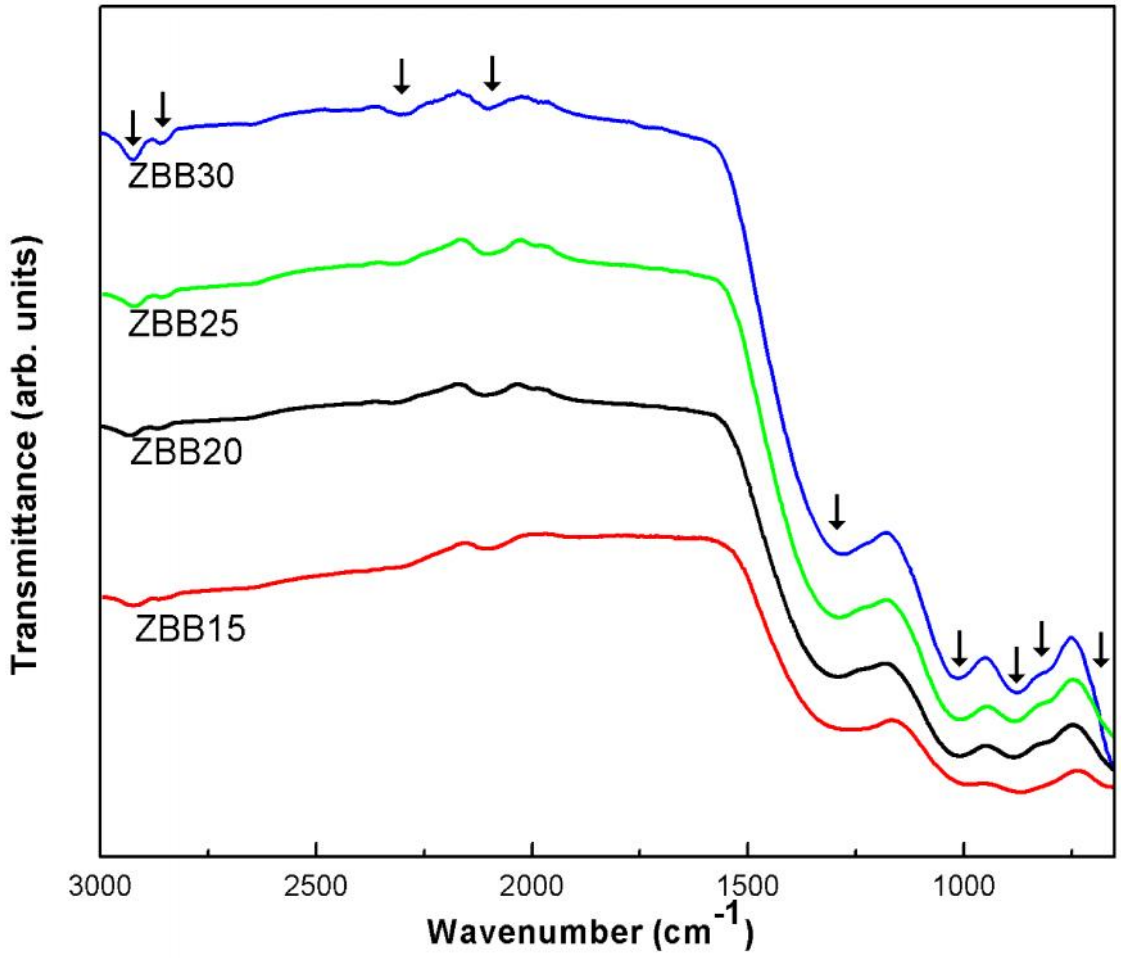

Figure 4.10 The IR transmission spectra of the xBi_2O_3 - 10ZnO - (90 - x) B_2O_3 (ZBB) glass system.

Table 4.4 FTIR analysis of the xBi_2O_3 : 10ZnO : (90 - x) B_2O_3 (ZBB) glass system.

Wavenumber (cm^{-1})	**IR band assignments**
651	The bending vibrations of B-O-B linkages of BO_3 units
766	The bending mode of =B-O-B≡ bonds
848	Symmetrical stretching vibration of the Bi-O bonds in the BiO_3 groups
966	Stretching vibrations of B-O bonds in BO_4 tetrahedral units
1,268	Asymmetrical stretching vibration of the B-O bonds in the trigonal units
2,080 – 2,904	OH bending mode of vibration

4.1.6 UV - VIS Absorption Study

The optical absorption spectra of the ZBB glasses are shown in Figure 4.11. The absorption edge as observed in UV - VIS region [117]. The position of the fundamental absorption edge or cut-off wavelength in these glasses shifts from 423, 432, and 439 to 447 nm as the content of Bi_2O_3 increases from 15, 20 and 25 to 30 mol%, respectively. In the present glass system, the shift of the absorption edge or cut-off wavelength to longer wavelength with increase in Bi_2O_3 content are related to the progressive increase in the concentration of non-bridging oxygen (NBO) atoms. This increase in turn gives rise to a possible decrease in the (B - O - B) bridging oxygens (BO). The shift is attributed to the structural changes which are as a result of the differing site occupations, i.e., interstitial or substitutional, of the bismuth ion which add to the zinc borate matrix and modify the network. We assume that as the cation concentration increases, the bridging oxygens (BO) develop bonds with Bi^{3+} which in turn lead to the gradual breakdown of the glass network. This breakdown seems edge shifts to longer wavelengths, as Bi_2O_3content is increased from 15 to 30 mol %.

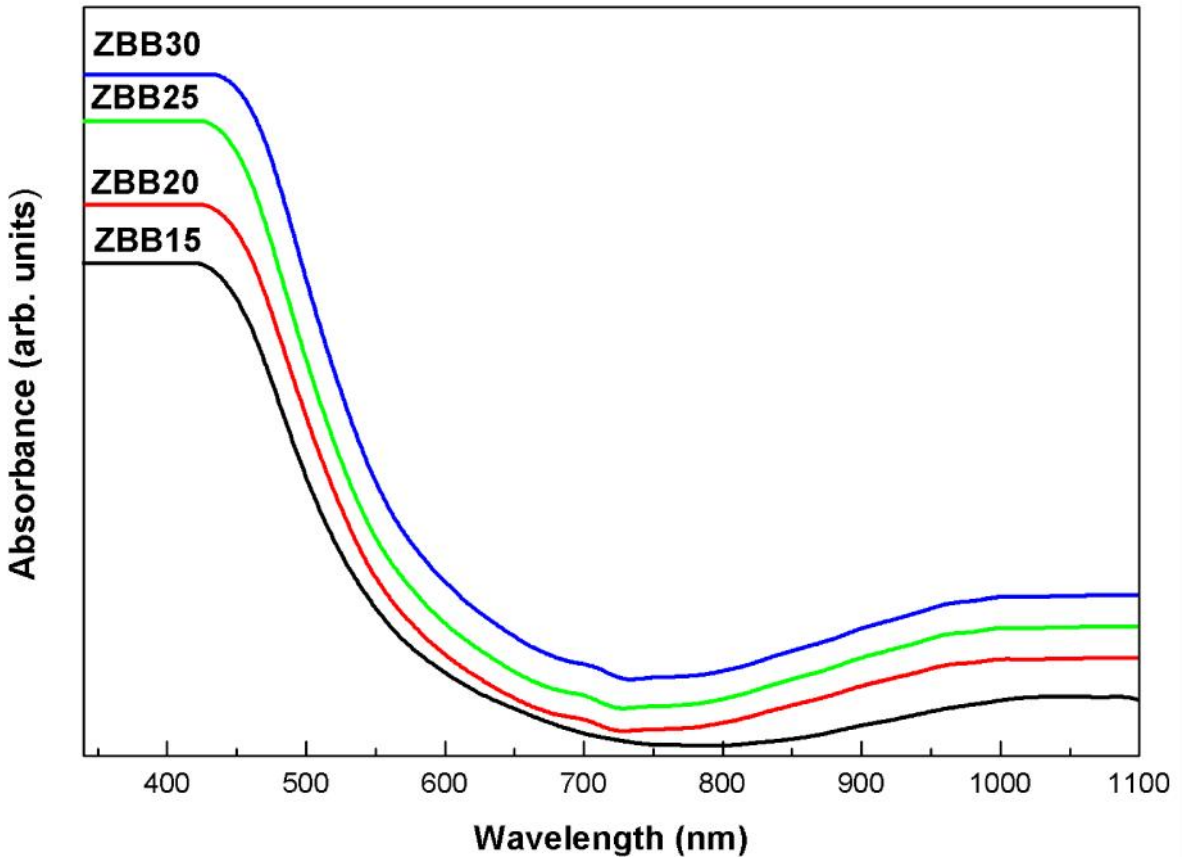

Figure 4.11 Optical absorption spectra of the ZBB glasses doped with different Bi_2O_3 concentrations.

4.1.7 Luminescence Spectra

According to experiments with Bi^{3+} doped glasses [118] also Bi^{3+} shows strong broad band emission even leading to laser emission. Electronic configuration of Bi^{3+} is *[Xe] $4f^{14}$ $5d^{10}$ $6s^2$*. The ground state is $^1S_0$ with *$6s^2$* configuration, and the excited states from *6s6p* configuration are $^3P_0$, $^3P_1$, $^3P_2$ and $^1P_1$ in a sequence of energy increasing. The transitions $^1S_0 \rightarrow {}^3P_0$ or $^3P_2$ are spin forbidden and $^1S_0 \rightarrow {}^3P_1$ or $^1P_1$ are lifted by spin-orbit coupling. So, the latter two have relatively higher absorption strength than the former two [119]. A broad band can be seen from the excitation spectra in the near UV range, 300 - 357 nm [120] with its centre at 302 nm and several weak peaks in the range 570 - 630 nm. The emission spectra of ZBB glasses were measured at room temperature by exciting the samples at 302 nm using the xenon flash lamp and are shown in Figure 4.12. All the spectra exhibited an emission bands corresponding to the $^3P_1 \rightarrow {}^1S_0$ (602 nm; red), transitions. Figure 4.13 shows the partial energy level diagram of Bi^{3+} in the ZBB glasses. When the Bi^{3+} are excited to level above the $^3P_1$ and the emission takes place from $^3P_1$ level to lower levels, $^1S_0$.

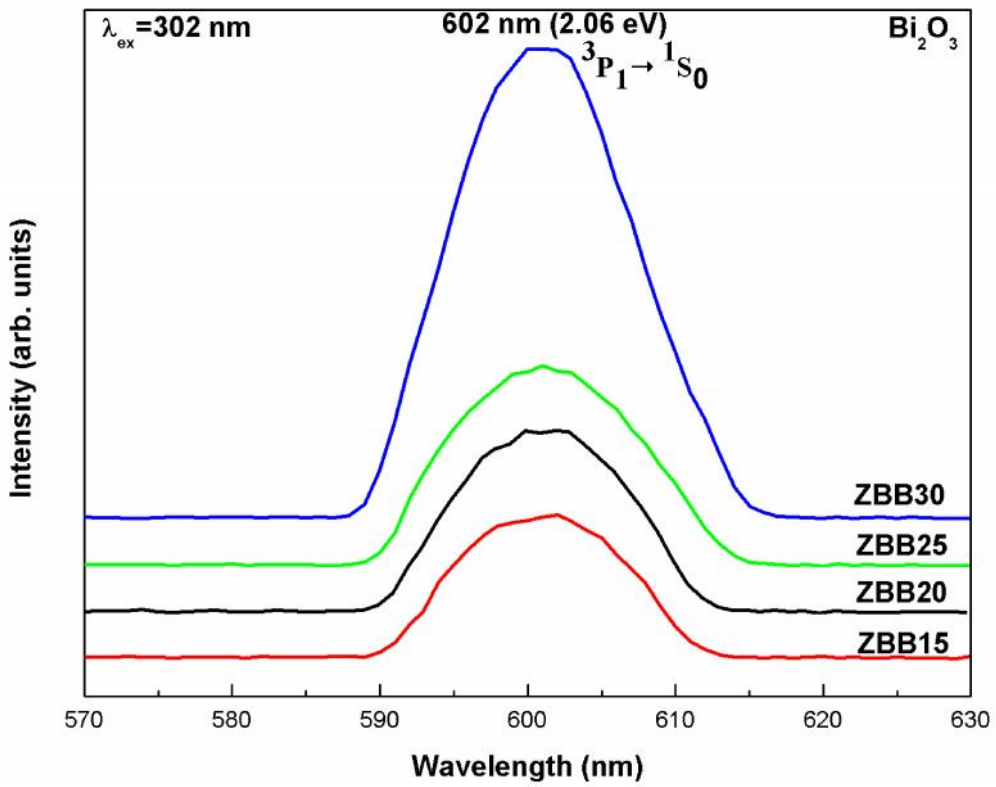

Figure 4.12 Luminescence spectra of the ZBB glasses doped with different Bi_2O_3 concentrations when excited with 302 nm at room temperature.

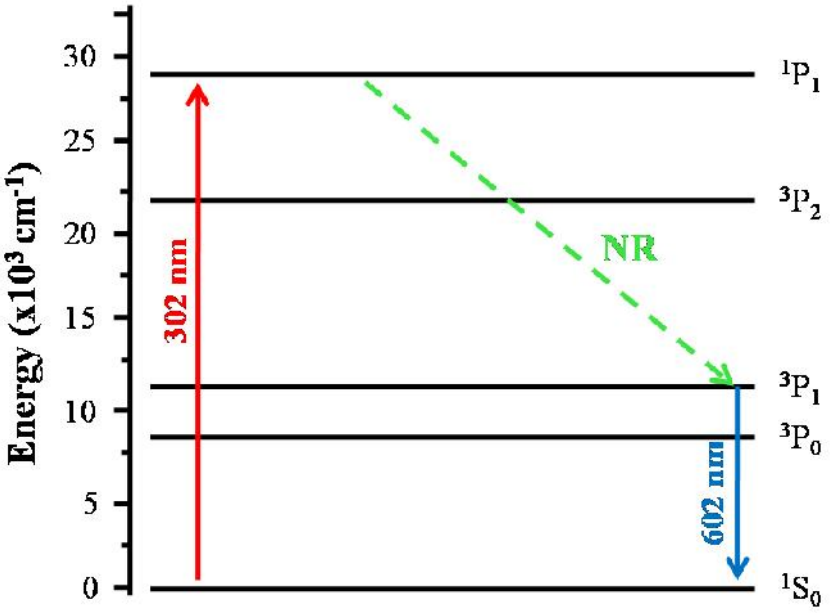

Figure 4.13 The Schematic energy levels diagram and possible transition pathways of Bi^{3+} ion.

4.1.8 Lifetime Profiles

Figure 4.14 shows the lifetime profiles of $^3P_1$ level for different Bi^{3+}concentrations in the ZBB glasses obtained by exciting the samples with 302 nm wavelength and by monitoring the emission at 602 nm. All the lifetime profiles are well fitted to single exponential function [121]. The measured lifetime (τ) obtained by taking the first e-folding times of the lifetime curves are 1201, 2005,2093 and 2247 μs for 15, 20, 25 and 30 mol % of Bi^{3+} doped ZBB glasses, respectively. The τ values slightly increases with Bi^{3+} concentration.

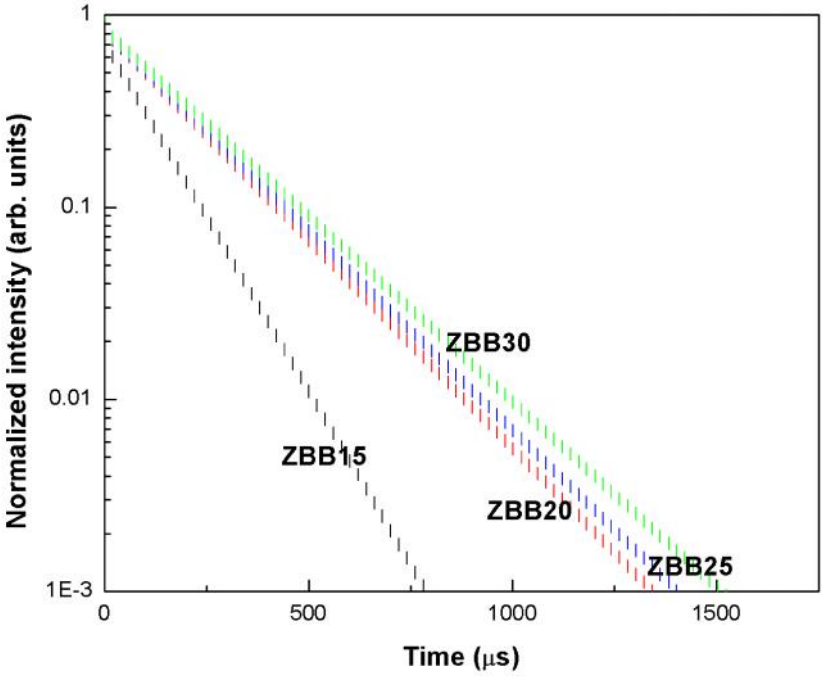

Figure 4.14 The lifetime profiles of $^3P_1$ level of Bi^{3+} : ZBB glasses.

4.1.9 Color of Glass Samples

Figure 4.15 shows the color of glasses were confirmed by CIE L*a*b* color coordinate and the brightness (L*) were decreased with the increasing of Bi_2O_3 content.

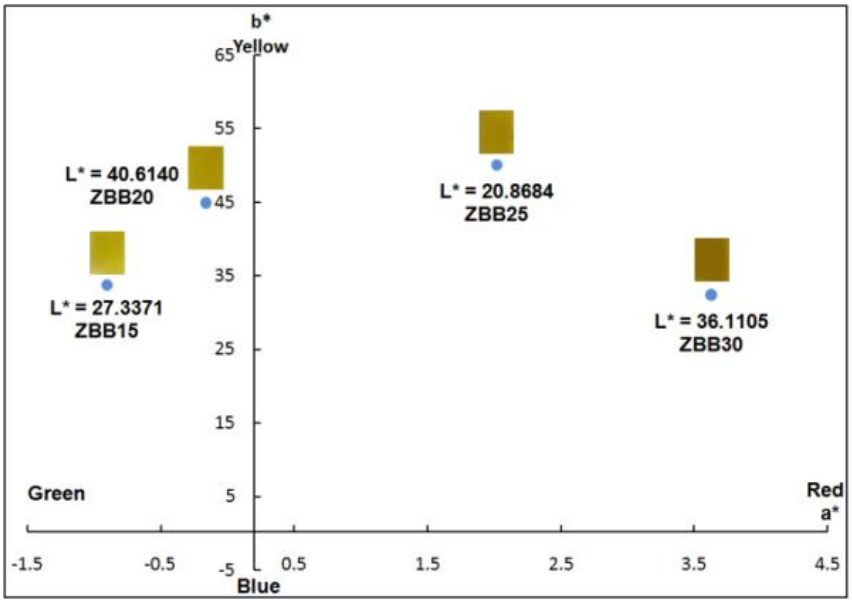

Figure 4.15 The color measurement of ZBB glasses in CIE *a*b* color scale.

4.2 Eu^{3+} Ion Doped in Zinc Bismuth Borate (ZBB) Glass Samples

4.2.1 General Characteristic of Glass Samples

The Eu^{3+}: ZBB glasses of chemical composition of (in mol %) (60 - x)B_2O_3 : 30Bi_2O_3 : 10ZnO : xEu_2O_3 (where x = 0.0, 0.2, 0.4, 0.6, 0.8 and 1.0 mol %) were prepared by a melt quenching technique. Chemical powers of analytical reagent consisted of ZnO, Bi_2O_3, H_3BO_3 and Eu_2O_3. All chemical composition was finely powder and then mixed in whole of composite. Batches for producing 30 g of glass were melted in high alumina crucibles in an electric furnace at 1,100 $^{\circ}$C with soaking time for 3 hours under normal atmospheric conditions. Afterwards, the melts were quickly poured onto a preheated stainless steel plate and pressed to a thickness of approximately 0.5 mm by another plate, annealed at 500 $^{\circ}$C for 3 hours, and slowly cooled down to room temperature, respectively. Finally, the as-prepared glass samples were cut and then finely polished to a dimension of 1.0 cm x 1.5 cm x 0.3 cm. The chemical compositions of Eu^{3+} : ZnO - Bi_2O_3 - B_2O_3 (ZBB) glasses prepared in the present study are given in Table 4.5. The photographs of ZBB glass samples with different concentrations of Eu^{3+} from 0.0 to 1.0 mol % are illustrated in Figure. 4.16. All the glass samples obtained are transparent and have good optical quality. Due to the homogeneous distribution of Bi^{3+} ion in the glass matrices, these glasses were found to be of its characteristic yellow in color.

Table 4.5 Fractional doping of Eu_2O_3 for zinc bismuth borate glass.

Samples no.	Eu_2O_3 (mol%)	Glass formula
1	0.0	30Bi_2O_3-60.0B_2O_3 -10ZnO
2	0.2	30Bi_2O_3-59.8B_2O_3 -10ZnO-0.2Eu_2O_3
3	0.4	30Bi_2O_3-59.6B_2O_3 -10ZnO-0.4Eu_2O_3
4	0.6	30Bi_2O_3-59.4B_2O_3 -10ZnO-0.6Eu_2O_3
5	0.8	30Bi_2O_3-59.2B_2O_3 -10ZnO-0.8Eu_2O_3
6	1.0	30Bi_2O_3-59.0B_2O_3 -10ZnO-1.0Eu_2O_3

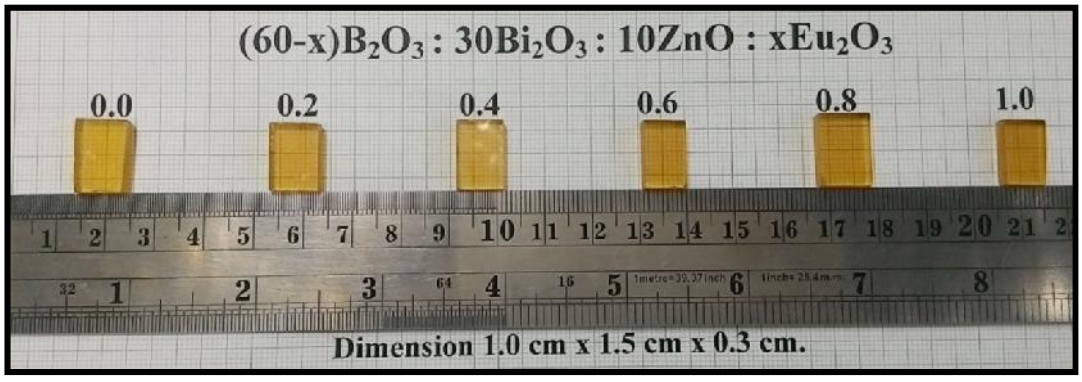

Figure 4.16 Photographs of ZBB glasses doped with different Eu_2O_3 concentrations.

4.2.2 Density, Molar Volume and Vicker's Hardness of glass samples

The density$(^\circ)$ and molar volume(V_M) of ZBB glasses doped with different Eu_2O_3 concentrations are shown in Table 4.6. Density of glass, in general, is explained in terms of competition between the masses and volumes of the various structural groups present in it. Therefore, density is related to how tightly the atoms and atomic groups are placed together in the glass network. The variations of density and hardness (in Vicker's scale) with composition of Eu_2O_3 are shown in Figures 4.17 and 4.18, respectively. The behavior of molar volume mainly depends on the density of glasses and as expected in the present case, it follows a trend opposite to density. The molar volumes of glasses were decreased with increasing of Eu_2O_3 concentration, reflecting that the glass structure was compactness with higher concentration of Eu_2O_3, which leads to decrease average atomic separation.

Table 4.6 The values of density ($^\circ$), molecular weight (M_T) and molar volume (V_M) of ZBB glasses doped with different Eu_2O_3 concentrations.

Sample No.	Glass formula (mol %)	Density $^\circ$ (g/cm^3)	Molecular weight M_T (g/mol)	Molar volume V_M (cm^3/mol)
1	$30Bi_2O_3$-$60.0B_2O_3$-10ZnO	3.5836±0.0023	189.69	52.9315
2	$30Bi_2O_3$-$59.8B_2O_3$-10ZnO-$0.2Eu_2O_3$	3.7988±0.0019	190.25	50.0816
3	$30Bi_2O_3$-$59.6B_2O_3$ -10ZnO-$0.4Eu_2O_3$	3.8477±0.0031	190.82	49.5919
4	$30Bi_2O_3$-$59.4B_2O_3$ -10ZnO-$0.6Eu_2O_3$	3.9882±0.0024	191.38	47.9864
5	$30Bi_2O_3$-$59.2B_2O_3$ -10ZnO-$0.8Eu_2O_3$	4.0439±0.0033	191.94	47.4650
6	$30Bi_2O_3$-$59.0B_2O_3$ -10ZnO-$1.0Eu_2O_3$	4.1295±0.0027	192.51	46.6178

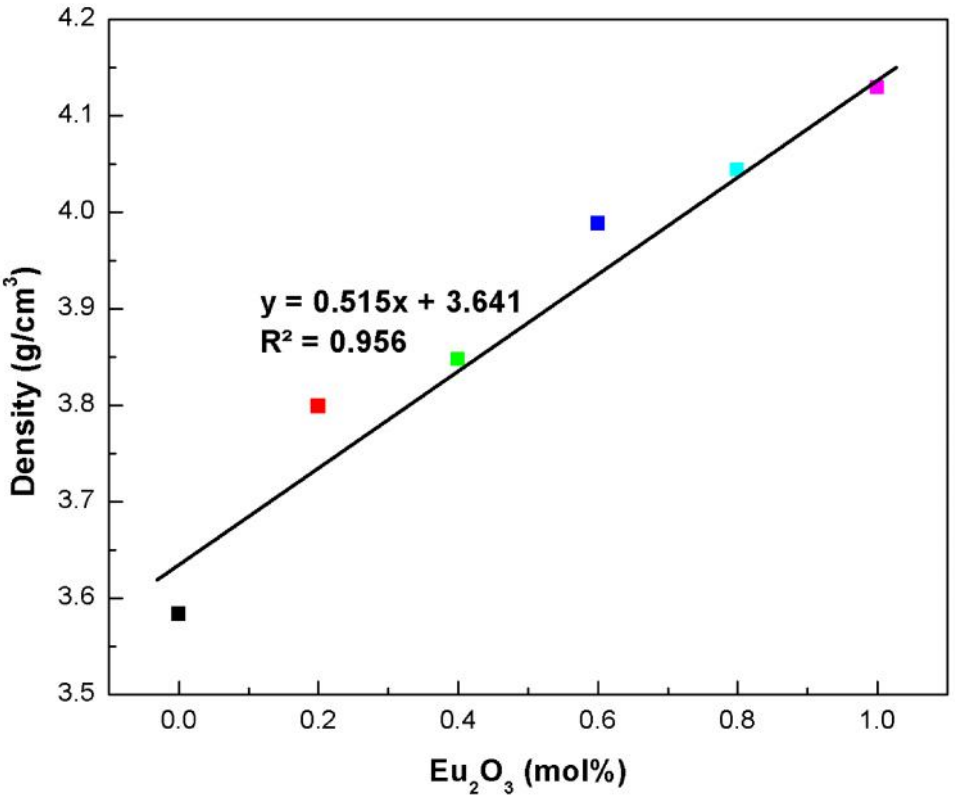

Figure 4.17 Densities of ZBB glasses doped with different Eu_2O_3 concentrations.

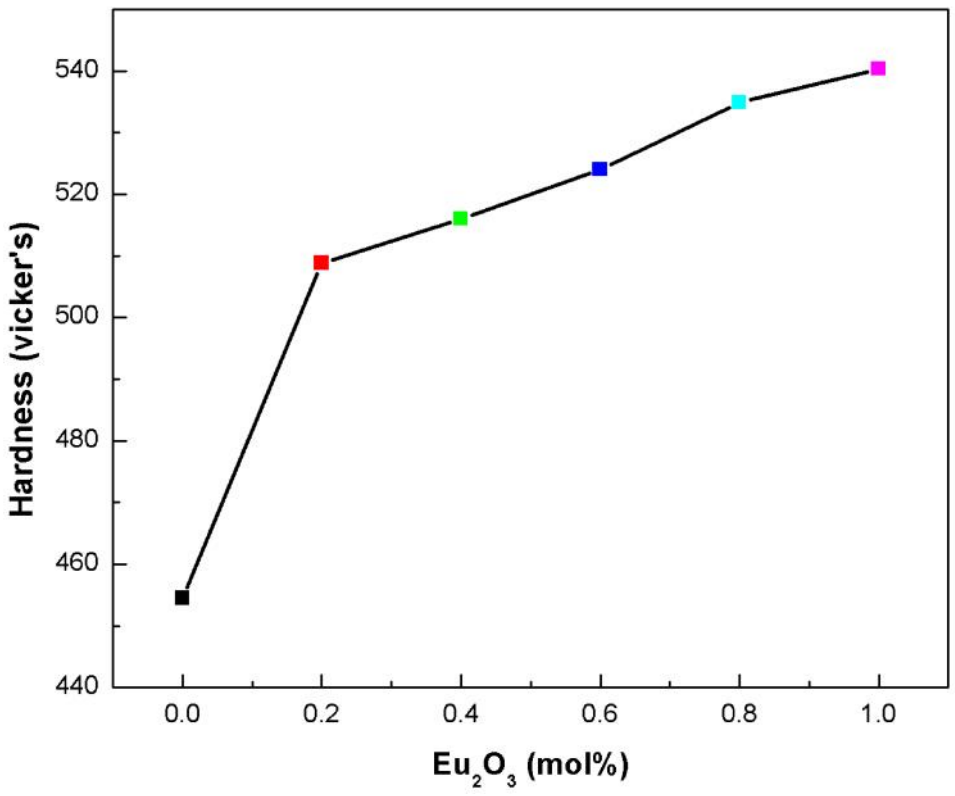

Figure 4.18 Vicker's hardness of ZBB glasses doped with different Eu_2O_3 concentrations.

4.2.3 Amorphous Nature of Glass Samples

The amorphous nature of ZBB glasses doped with different Eu_2O_3 concentrations was confirmed by X - ray diffractometer from Cu (K_α, λ = 1.5406 Å) with an angular range 20 - 80 (2θ) degree with a step length of 0.02 degree and a counting time 60 sec/step. X - ray diffraction patterns of all glass samples show a hump were observed in the 2θ about 30 degree, indicating disordered structure and amorphous nature of glass samples. The XRD patterns of ZBB glasses doped with different Eu_2O_3 concentrations are shown in Figure 4.19.

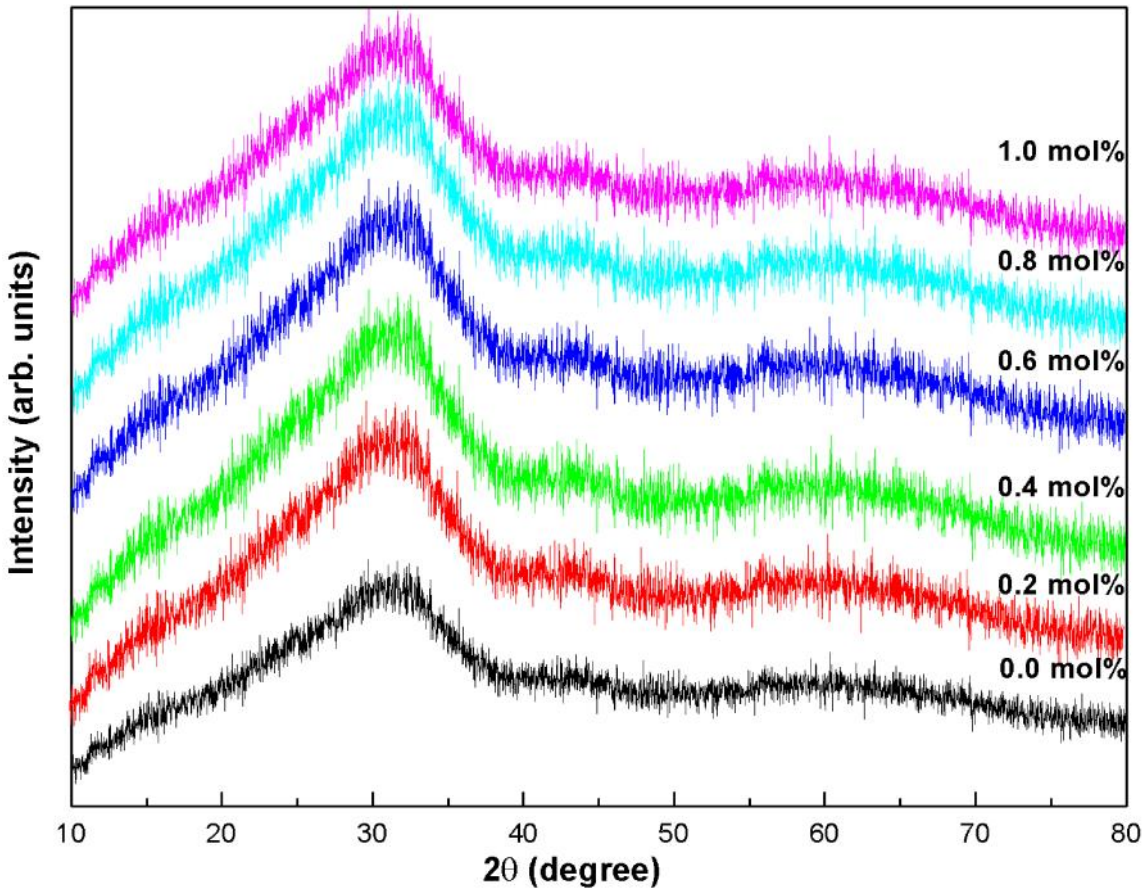

Figure 4.19 Diffraction patterns of ZBB glasses doped with different Eu_2O_3 concentrations.

4.2.4 FTIR Transmittance Spectra

The infrared spectra of (60 - x)B_2O_3 : 30Bi_2O_3 : 10ZnO : xEu_2O_3 glass system (where x = 0.0, 0.2, 0.4, 0.6, 0.8 and 1.0 mol %) is displayed in Figures 4.20. According to Krogh - Moe model, the structure of borate glass consists of BO_3 triangles with certain fraction of six membered (boroxol) rings [105]. In B_2O_3 glasses boron [B^{3+}] ion are triangularly coordinated by oxygen to form glasses easily. The BO_3 triangles are corner bonded in a random network [106]. The introduction of transition metal ions in these glasses helps the boron to form tetraborate groups and progressive substitution of boroxal rings by triborate and tetraborate groups [107]. The boroxal ring shows its characteristic frequency at 806 cm^{-1} and the presence or absence of this band decides the existence or absence of boroxal rings in the structure. In the present set of glasses no band was observed at or around 806 cm^{-1} indicating that no boroxol rings are present in these glasses.

The peaks of the IR spectra of the glasses under study are listed in Table 4.7. The bands observed in the region 2080 - 2940 in all the glass samples are attributed to the hydroxyl or water group [108]. The present set of glasses show transmission bands in regions 2904, 2830, 2287, 2080, 1268, 996, 848, 766 and 651 cm^{-1}. It has been reported that the bands observed in the region 1268 cm^{-1} are due to the asymmetrical stretching relaxation of the B - O bond of trigonal BO_3 units [109]. The band around 996 cm^{-1} originates from B - O bond stretching of the tetrahedral BO_4 units and is due to the vibration of some boron atoms attached to the non-bridging oxygen in the form of BO_4 vibrations [110]. The shoulder around 840 cm^{-1} is related to the symmetrical stretching vibration of Bi - O in [BiO_3] group [111]. The band around 766 cm^{-1} is the bending mode of = B – O – B ≡ bonds in which oxygen bridges between one tetrahedral and one trigonal boron atom [112]. The band observed around 651 cm^{-1} is the bond bending mode of B - O - B vibrations [113-114]. In the IR spectra of the present glass system it was found that the incorporation of ZnO does not show much effect on the structure of the glasses under study. The addition of ZnO in the present glass system produces a very small change in the IR bands that do not account for the major structural changes. However, in many glass systems in which ZnO is a major constituent the possibility of formation of ZnO_4 may be more [115]. S. Bale et al. have reported the formation of ZnO_4 units with increase in zinc oxide content [116].

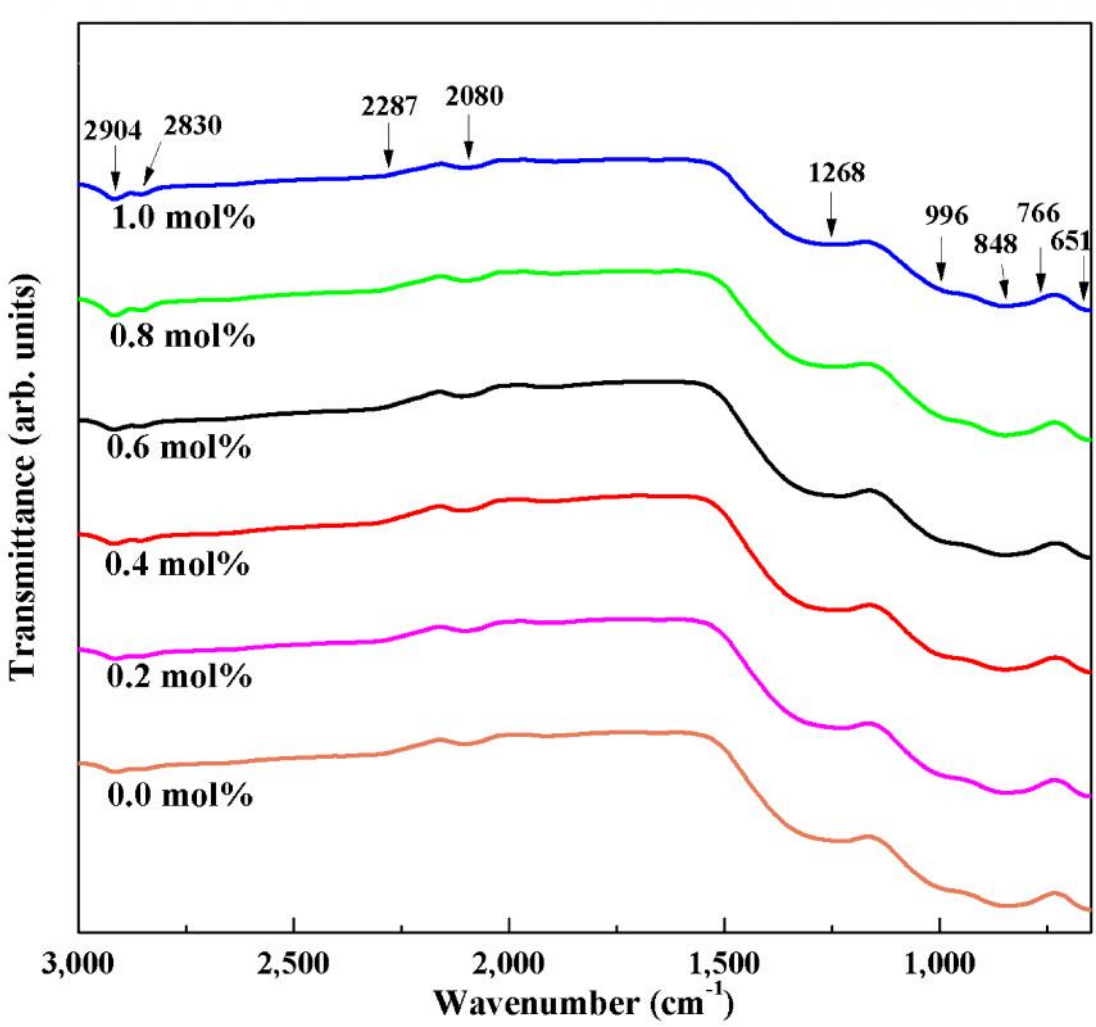

Figure 4.20 The IR transmission spectra of ZBB glasses doped with different Eu_2O_3 concentrations.

Table 4.7 FTIR analysis of the (60 - x)B_2O_3 : 30Bi_2O_3 : 10ZnO : xEu_2O_3 glass system.

Wavenumber (cm^{-1})	IR band assignments
651	The bending vibrations of B-O-B linkages of BO_3 units
766	The bending mode of =B-O-B≡ bonds
848	Symmetrical stretching vibration of the Bi-O bonds in the BiO_3 groups
966	Stretching vibrations of B-O bonds in BO_4 tetrahedral units
1,268	Asymmetrical stretching vibration of the B-O bonds in the trigonal units
2,080 – 2,904	OH bending mode of vibration

4.2.5 UV - VIS - NIR Absorption Study

The absorption spectrum of the ZBB glasses doped with different Eu_2O_3 concentrations in NIR regions (1800 - 2400 nm) is shown in Figure 4.21 along with the assignments of the absorption bands. The assignment of energy levels has been done according to Carnall et al. [119]. The absorption spectra revealed two intense bands due to $^7F_0 \rightarrow {}^7F_6$ (2076 nm) and $^7F_1 \rightarrow {}^7F_6$ (2198 nm) transitions in the NIR regions. It is well known that except for Eu^{3+} ion, all the other trivalent RE $^{3+}$ ions posses single populated ground state. The close examination of absorption band positions of $^7F_0 \rightarrow {}^7F_6$ and $^7F_1 \rightarrow {}^7F_6$ transitions clearly indicates that the energy gap between the ground state ($^7F_0$) and the first excited state ($^7F_1$) is about ~360 cm^{-1}. Due to the effect of thermalization, the fractional population of any excited level is given by Van Deun et al. [120].

$$(C_J / C_0) = (g_J / g_0) e^{-(E_J - E_0)/kT} \tag{4.2}$$

where C_0, C_J, E_0, E_J, g_0 and g_J (2J + 1) are the thermal correction factors, energies and degeneracies for the ground state ($^7F_0$) and the first excited state ($^7F_1$), respectively. The magnitude of *k*T is the order of 208 cm^{-1}, where k is the Boltzmann's constant and T is the absolute room temperature (300 K). For the ZBB glasses doped with different Eu_2O_3 concentrations, the evaluated thermal correction factors for the ground state ($^7F_0$) and the first excited state ($^7F_1$) are: C_0 = 0.65 and C_1 = 0.35, respectively. Owing to the population of $^7F_0$ (~ 65%) and $^7F_1$ (~ 35%) states, the absorption spectrum exhibited the transitions originating not only from the ground level ($^7F_0$), but also from the first excited level ($^7F_1$).

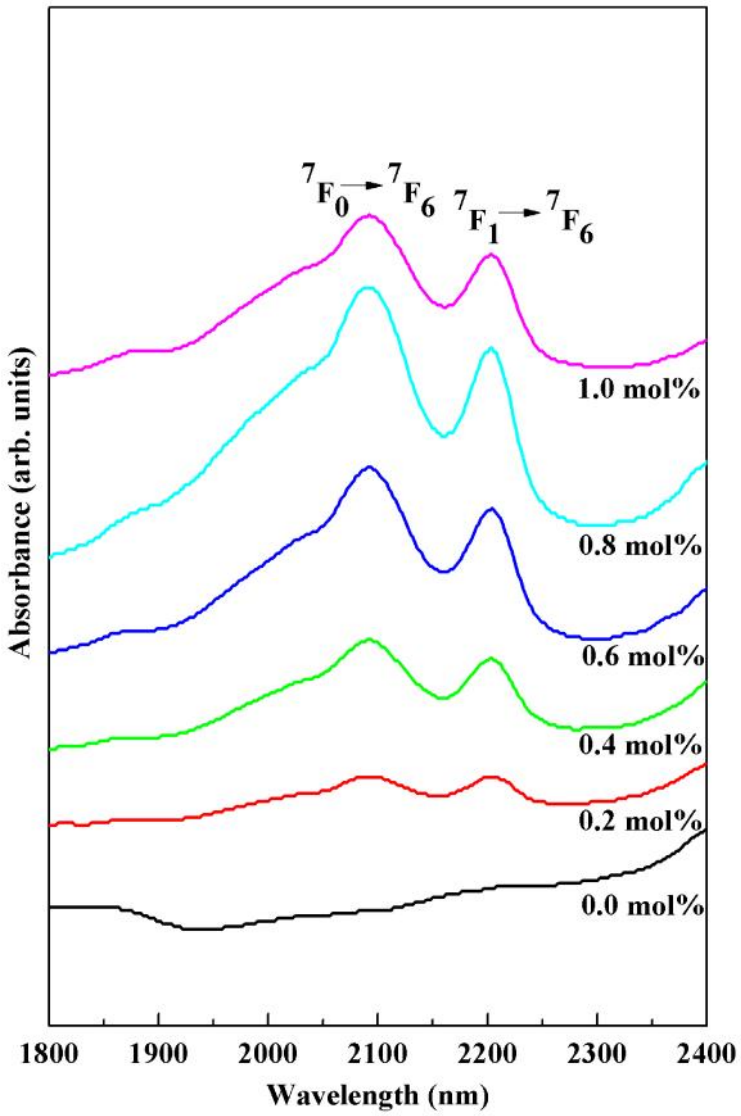

Figure 4.21 Optical absorption spectra of the ZBB glasses doped with different Eu_2O_3 concentrations.

4.2.6 Luminescence Spectra

The luminescence spectra of Eu^{3+} : ZBB glasses were measured from 520 - 720 nm at room temperature by exciting the samples at 465 nm using the xenon flash lamp and is shown in Figure 4.22. All the spectra exhibited five emission bands corresponding to the $^5D_0 \rightarrow {}^7F_0$ (579 nm; yellow), $^5D_0 \rightarrow {}^7F_1$ (589 nm; orange), $^5D_0 \rightarrow {}^7F_2$ (613 nm; red), $^5D_0 \rightarrow {}^7F_3$ (651 nm; deep-red) and $^5D_0 \rightarrow {}^7F_4$ (696 nm; deep - red) transitions Figure 4.23 shows the partial energy level diagram of Eu^{3+} ion in the ZBB glasses along with emission and non - radiative (NR) channels. When the Eu^{3+} ion is excited to any level above the $^5D_0$, there is a fast non - radiative multiphonon relaxation to $^5D_0$ level [124] and the emission takes place from $^5D_0$ level to lower levels, ^7F_J.

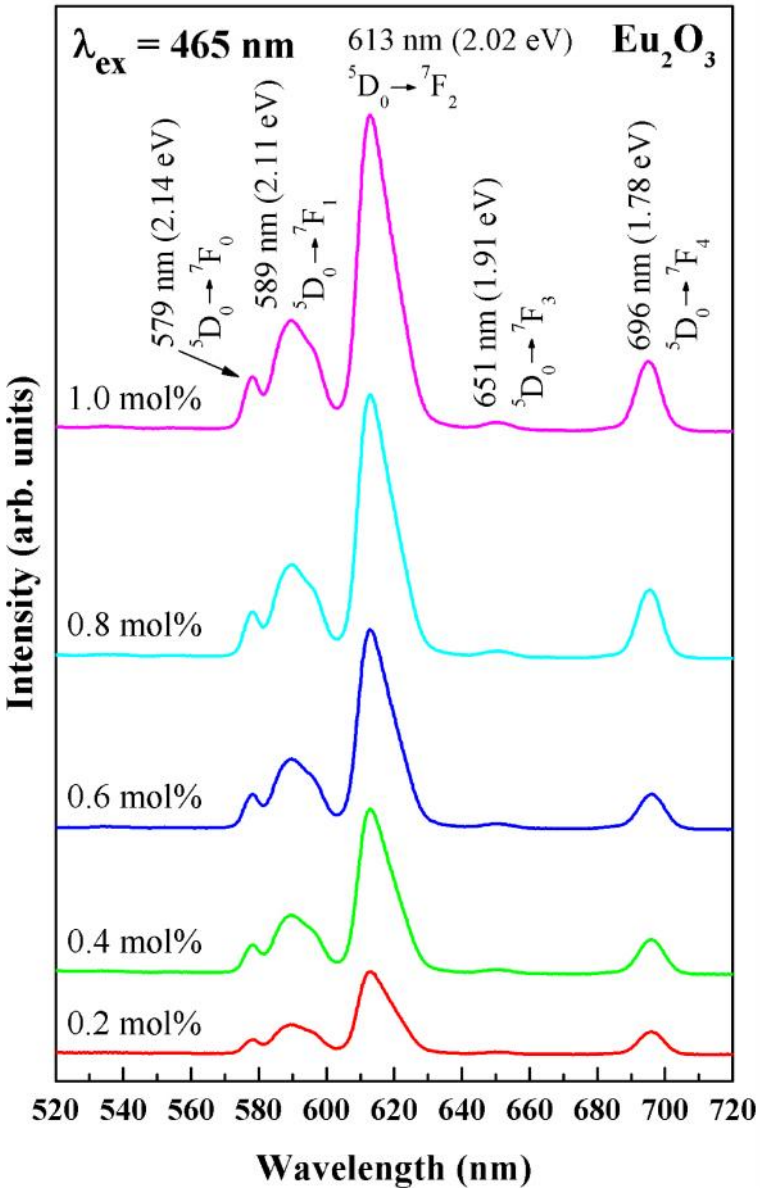

Figure 4.22 Luminescence spectra of the ZBB glasses doped with different Eu_2O_3 concentrations when excited with 465 nm at room temperature.

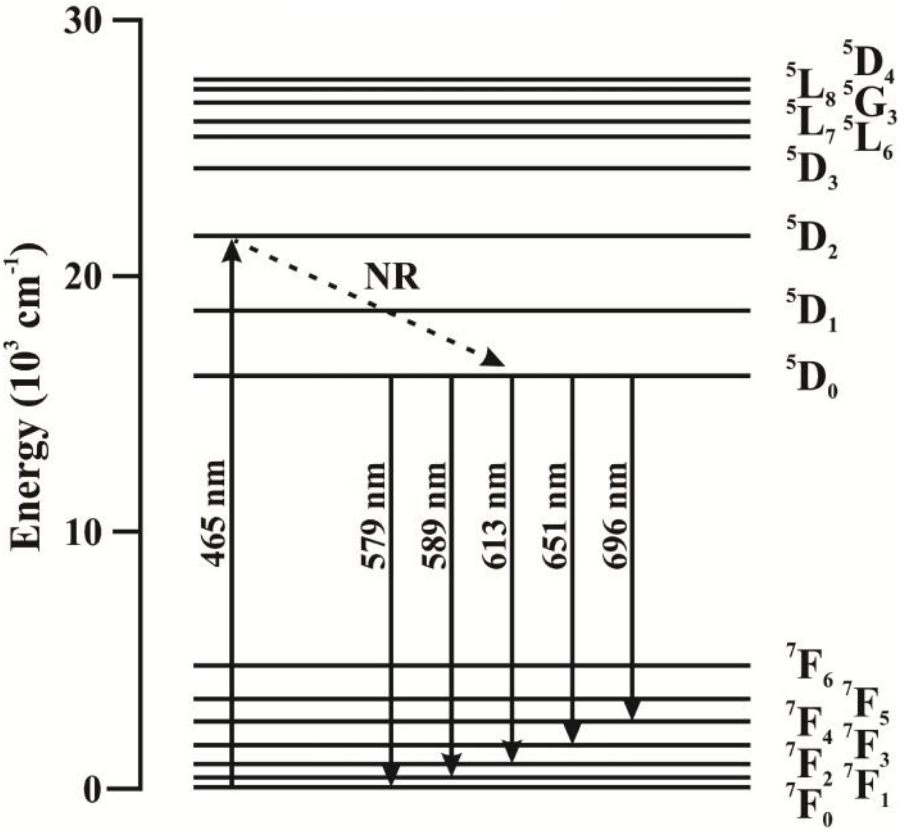

Figure 4.23 The schematic partial energy levels diagram and possible transition pathways of Eu^{3+} ion.

4.2.7 Lifetime Profiles

Figure 4.24 shows the lifetime profiles of $^5D_0$ level for different Eu^{3+} concentrations in the ZBB glasses obtained by exciting the samples with 465 nm wavelength and by monitoring the emission at 613 nm. All the lifetime profiles are well fitted to single exponential function, $I_t = I_o^{e-t/\tau}$, where I_o is the fluorescence intensity when $t = 0$ and (τ) represents the lifetime of the excited state. The measured lifetimes (τ) obtained by taking the first e - folding times of the lifetime curves are 64, 105, 295, 478 and 621 μs for 0.2, 0.4, 0.6, 0.8 and 1.0 mol % of Eu^{3+} doped ZBB glasses, respectively. The lifetime values slightly increases with Eu^{3+} concentrations.

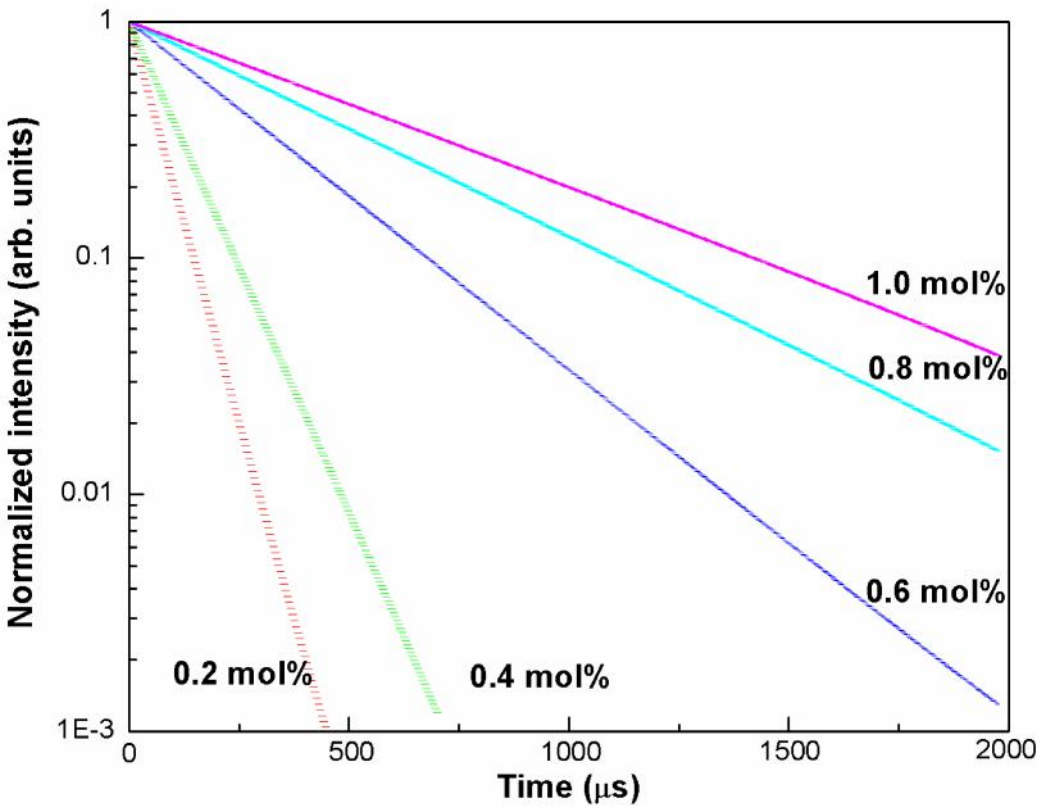

Figure 4.24 The lifetime profiles of $^5D_0$ level of Eu^{3+} : ZBB glasses.

4.2.8 Color of Glass Samples

The Commission International De I - Eclairage (CIE) 1931 chromaticity coordinates for ZBB glasses doped with different Eu_2O_3 concentrations as a function of Eu^{3+} ion for the luminous color was depicted by the emission spectra. The CIE chromaticity coordinates calculated from the emission spectra were shown in Figure 4.22. According to our knowledge, the CIE coordinates of red emission of Eu^{3+} ion not only depend upon the asymmetric ratio but also depend upon the higher energy ^5D_J (= 3, 2, 1) emission levels [122]. The corresponding emission spectra were converted to the CIE 1931 chromaticity diagram as shown in Figure 4.25. It can be observed, that the location was marked in Figure 4.20 with circle in red orange region. The color coordinates for ZBB glasses doped with different Eu_2O_3 concentrations are x = 0.64411, 0.64439, 0.64491, 0.64583and 0.64535; y = 0.35412, 0.35388, 0.35396, 0.35336 and .35366 with x and y = 0.0, 0.2, 0.6, 0.8, and 1.0 mol%, respectively (these coordinates are very near to the red - orange light emission). Hence this phosphor having excellent color tenability from orange to red orange light emission.

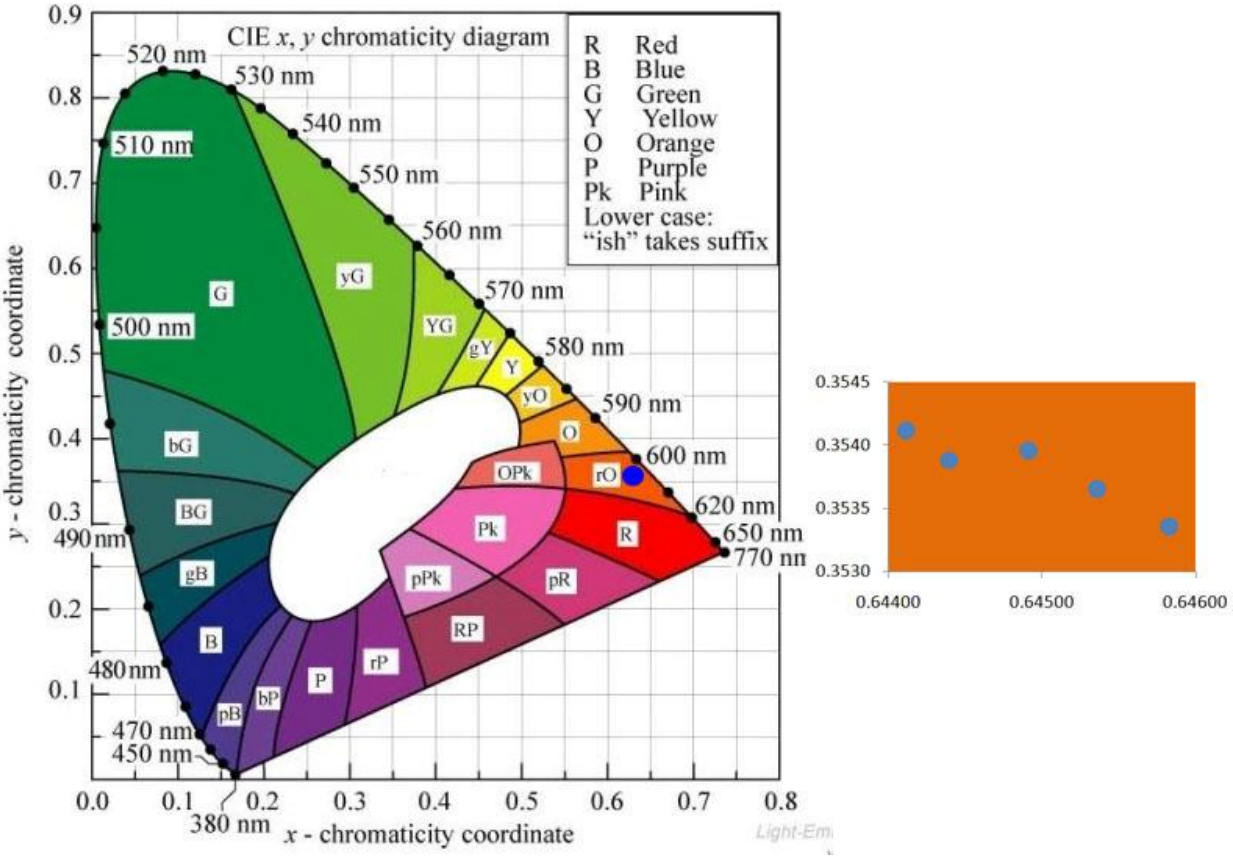

Figure 4.25 The CIE diagram of ZBB glasses doped with different Eu_2O_3 concentrations.

4.2.9 X-ray Luminescence

Figure 4.26 shows the X - ray luminescence spectra of different Eu_2O_3 concentration doped in zinc bismuth borate glass at room temperature. All samples emitted a luminescence with the emission peaks at 589 nm, 613 nm and 696 nm. The emission spectra peaks were due to the $^5D_0 \rightarrow {}^7F_0$ (589 nm), $^5D_0 \rightarrow {}^7F_2$ (613 nm) and $^5D_0 \rightarrow {}^7F_0$ (696 nm) respectively. The X - ray luminescence intensities of peak at 613 nm are slightly increased with increasing of Eu_2O_3 concentration and the strongest intensity peak at 613 nm was obtained, similar with photoluminescence results. The X - ray luminescence process of Eu^{3+} in (60 - x)B_2O_3 : 30Bi_2O_3 : 10ZnO : xEu_2O_3 glasses is shown in Figure 4.28.

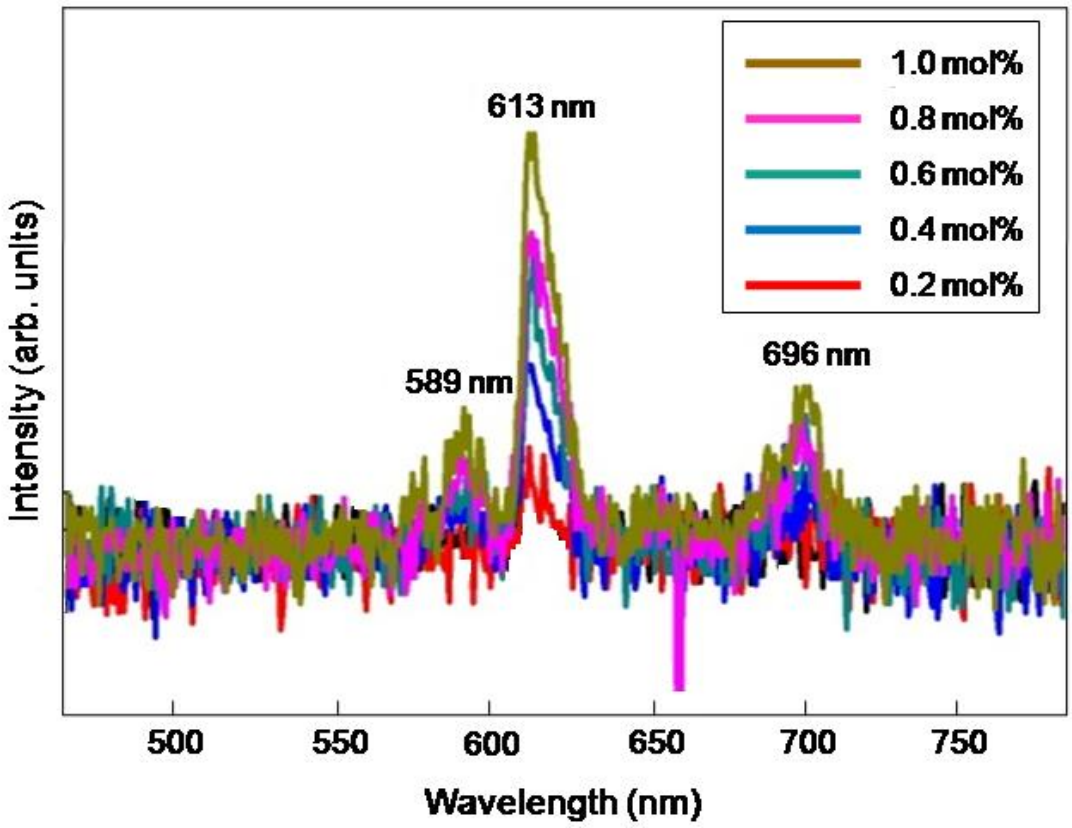

Figure 4.26 The X - ray luminescence spectra (60 - x)B_2O_3 : 30Bi_2O_3 : 10ZnO : xEu_2O_3 glasses.

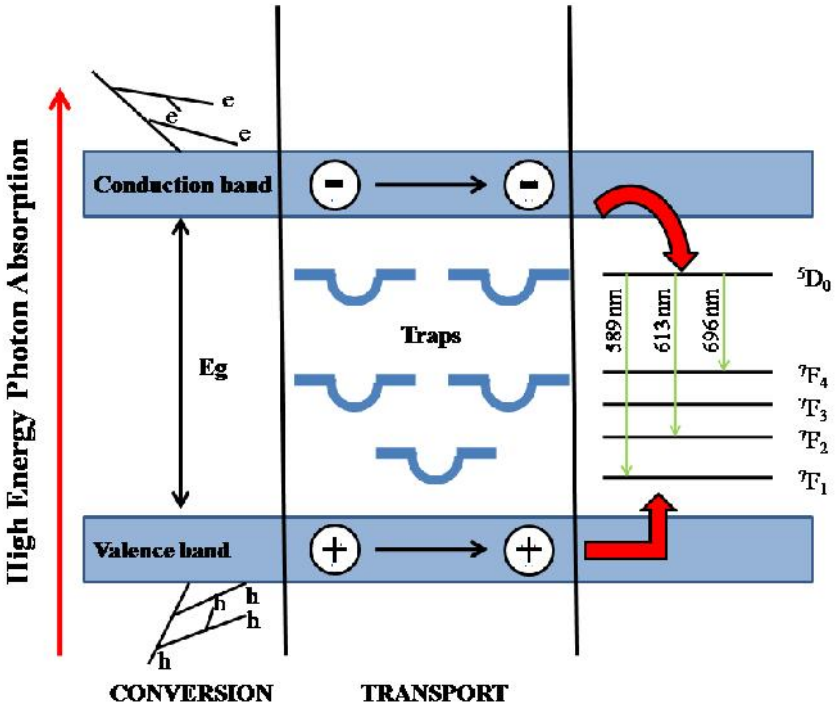

Figure 4.27 X - ray luminescence process of Eu^{3+} $(60 - x)B_2O_3 : 30Bi_2O_3 : 10ZnO : xEu_2O_3$ glasses (adapted from [123]).